Nuclear Instruments and Methods in Physics Research A 652 (2011) 387–391

Contents lists available at ScienceDirect

Nuclear Instruments and Methods in Physics Research A

journal homepage: www.elsevier.com/locate/nima

Enhanced variant designs and characteristics of the microstructured solid-state neutron detector

S.L. Bellinger [a,*], R.G. Fronk [a], W.J. McNeil [a], T.J. Sobering [b], D.S. McGregor [a]

[a] S.M.A.R.T. Laboratory, Department of Mechanical and Nuclear Engineering, Kansas State University, Manhattan, KS 66506, USA
[b] Electronics Design Laboratory, Kansas State University, Manhattan, KS 66506, USA

ARTICLE INFO

Available online 8 September 2010

Keywords:
Semiconductor neutron detectors
Microstructured solid-state neutron detector
^{3}He replacement technology
Microstructured diode
Silicon wet-etching
Charge transport simulation

ABSTRACT

Silicon diodes with large aspect ratio perforated microstructures backfilled with ^{6}LiF show a dramatic increase in neutron detection efficiency beyond that of conventional thin-film coated planar devices. Described in this work are advancements in the technology with increased microstructure depths and detector stacking methods to increase thermal neutron detection efficiency. The highest efficiency devices thus far have delivered over 37% intrinsic thermal neutron detection efficiency by device-coupling stacking methods. The detectors operate as conformally diffused *pn* junction diodes with 1 cm^{2} square-area. Two individual devices were mounted back-to-back with counting electronics coupling the detectors together into a single dual-detector device. The solid-state silicon device operated at 3 V and utilized simple signal amplification and counting electronic components. The intrinsic detection efficiency for normal-incident 0.0253 eV neutrons was found by calibrating against a ^{3}He proportional counter and a ^{6}LiF thin-film planar semiconductor device. This work is a part of on-going research to develop solid-state semiconductor neutron detectors with high detection efficiencies and uniform angular responses.

1. Introduction

Microstructured semiconductor diode devices, backfilled with neutron reactive materials, have been suggested as high-efficiency thermal neutron detectors as far back as 1987 by Muminov and Tsvang [1] and more recently by Schelten et al. [2], Schelten and Reinartz [3], and Allier [4], with much enthusiastic investigative work completed in the last decade [5–28]. The basic configuration consists of a common *pn* junction diode, that is microstructured with an etched pattern, and then backfilled with neutron reactive materials. Such devices are compact, easily produced in mass-quantity, have low power requirements, and are far superior to common thin-film planar neutron detectors, which are restricted to low thermal neutron detection efficiencies, typically not greater than 4.5% intrinsic efficiency [29–33]. The relatively low efficiency of these planar devices, due to reaction product self-absorption in the neutron sensitive coating, makes them unpopular for common applications such as real-time dosimetry or area monitors. For this work, the neutron reactive material is based on the ^{6}Li(n,t)^{4}He reaction, such that when thermal neutrons are absorbed in ^{6}Li, a 2.73 MeV triton and a 2.05 MeV helium nucleus are ejected in opposite directions. In comparison to other neutron reactive materials, the reaction products from the ^{6}Li(n,t)^{4}He reaction are far more energetic than those of the ^{10}B(n,α)^{7}Li or ^{157}Gd(n,γ)^{158}Gd reactions, thereby improving detection and discrimination from measurable background radiations [7,26]. Therefore, the following work concentrates only on devices constructed with ^{6}LiF as the neutron converter material.

The present work employs the same technology, along with some new fabrication techniques to increase microstructure depths in the Si diode and stacking dual-integrated detectors to achieve unmatched solid-state neutron detection efficiency. With recent advancements in inductively coupled plasma-reactive-ion-etching (ICP-RIE) using high-aspect ratio deep etching (HARDE) techniques, along with common MEMS wet-etching techniques [2,4,34], unique neutron detector microstructures have been realized. Wet-etched strait trench microstructured diode devices (250 μm in depth) have been fabricated and backfilled with ^{6}LiF neutron absorber material (see Fig. 1). Two variations of the diodes have been previously fabricated, such that they either have a rectifying *pn* junction selectively formed around the etched microstructures or have *pn* junctions conformally diffused inside the microstructures [26, 27]. Conformal diffused devices have shown improved performance with more uniform electric fields in the detector active region [22]. Further discussion of the conformal diffused device modeled limitations will be presented.

The focus of this work involved mounting two detector chips back-to-back with counting electronics coupling them together into a single detector device. For the dual-detector device, the

* Corresponding author.
E-mail address: slb3888@ksu.edu (S.L. Bellinger).

0168-9002/$ - see front matter © 2010 Elsevier B.V. All rights reserved.
doi:10.1016/j.nima.2010.08.049

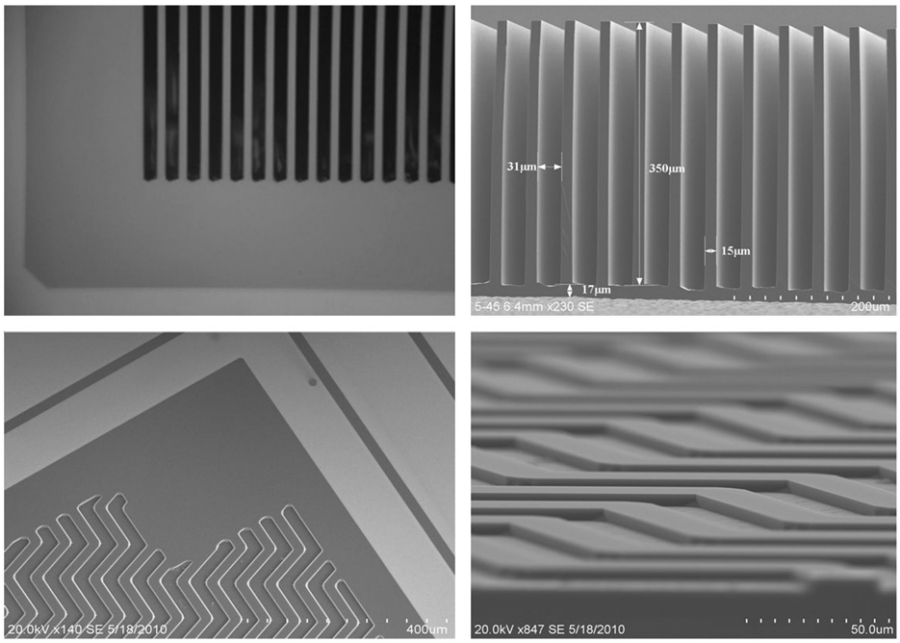

Fig. 1. Images of wet-etched strait- and chevron trench microstructured detectors. The upper left shows above-view of strait trench microstructure, the upper right shows a cleaved side view of high-selectivity deep-etched trenches, and the two bottom pictures show an above-view and side-view of chevron trench microstructures.

intrinsic detection efficiency for normal-incident 0.0253 eV neutrons was found, calibrated against thin-film planar semiconductor devices and a calibrated ^{3}He proportional counter. An important clear advantage for the 3D microstructured neutron detectors is the high efficiency achieved with a single device. Furthermore, these devices can be dual-integrated, by stacked configurations, into a single device to dramatically increase the counting efficiency of the neutron detector.

2. Microstructured neutron detector design

Initially, an oxide is grown on a 10 kΩcm *n*-type Si wafer, in which a diffusion window is patterned. Microstructured perforations are then etched into the Si diffusion windows with an ICP-RIE process or a KOH wet-etch process where the trench pattern is aligned to the ⟨1 1 1⟩ planes in a (1 1 0) orientated Si wafer. Individual detectors are batch processed on 3 in. diameter wafers, each with an active square-area of 1 cm^2. The devices reported in the present work have strait trenches etched 250 μm deep by 25 μm wide, where the trenches are periodically spaced 50 μm apart. The strait trench design maintains high neutron detection efficiency while creating an opportunity to off-set stack the detector chips so as to maximize neutron absorption as shown in Fig. 2. After the etch process, the wafer is chemically cleaned and *p*-type regions are diffused uniformly into individual device microstructures across the wafer, thereby forming *pn* junctions within the trenches. A Ti–Au metal contact is fabricated on the backside of the wafer to make an electrical ground contact, thereby completing the diode structure and enabling depletion through the bulk of the individual devices. Finally, ^{6}LiF powder is packed into the perforations to function as the neutron absorbing converter material.

Individual device chips are then mounted as dual-integrated detector systems. The dual-detector amplifying and readout electronics were specifically designed in-house and consists of a sandwiched detector board and a separate motherboard (see Figs 3 and 4). The separate motherboard configuration was used for research purposes as it simplifies testing multiple detector types through the use of common electronics. On the

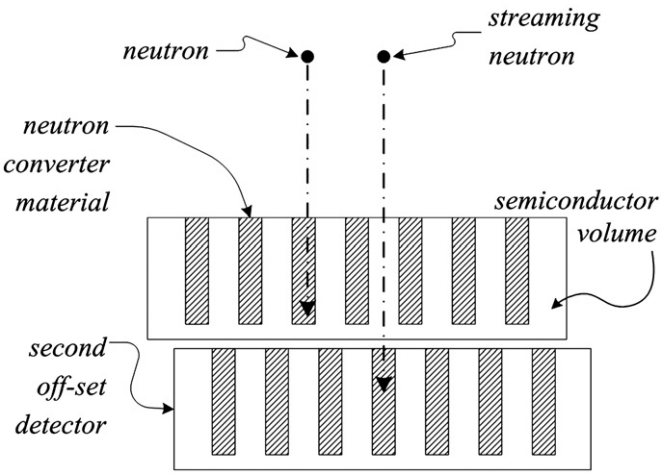

Fig. 2. Illustration of neutron efficiency gain from stacking second detector off-set from the first. Note that the 2200 m/s neutron absorption cross-section of silicon is small, $\sigma_{Si,a}=0.171$ b [35].

preamp board, a copper foil is sandwiched between two printed circuit boards that have an exposed backside plane. This provides the connection for the positive bias voltage to the detector cathodes. Two neutron detectors are mounted to a copper foil using conductive silver epoxy. On the front of the PC boards the detector anodes are wire-bonded to gold pads that are electrically connected by a post through the sandwiched boards. In this configuration, the anodes of each detector are common and applied to the input of a charge sensitive preamp with a ~10 μs time constant and a nominal gain of −1 mV/fC. A relatively short time constant is used because high counting rates are expected for some applications. The preamp board can be reconfigured such that feedback from a downstream integrator can be applied to compensate for the large leakage currents resulting from the trenching of the detectors. All connections to and from the preamp board are on a single row 10-pin edge connector.

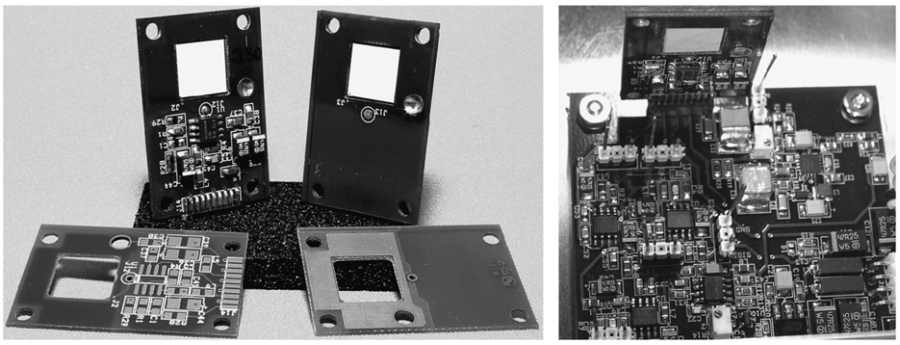

Fig. 3. Shown on the left are dual-integrated packaged devices with preamplifying circuitry. The right picture is of the motherboard, which provides an adjustable detector bias, bias current compensation, pulse shaping and gain, an analog output for pulse-height analysis, and a "digital" output from a discriminator.

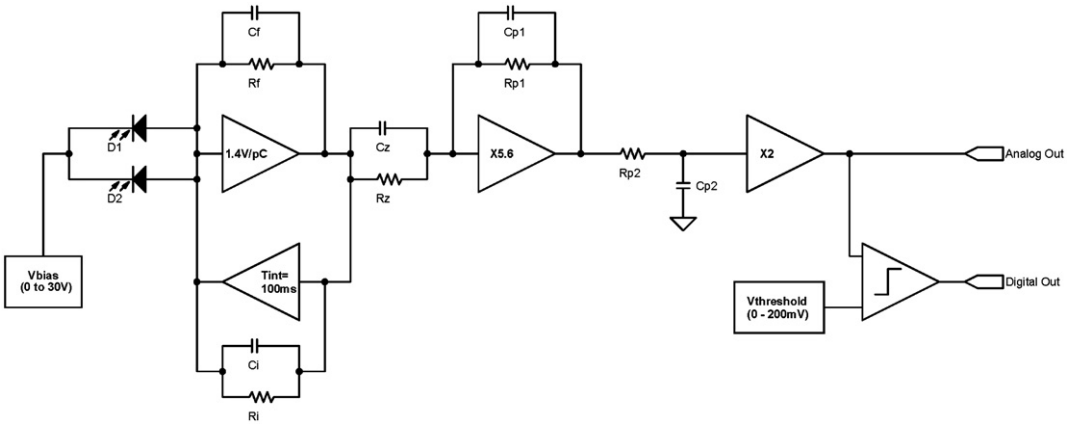

Fig. 4. Illustrated above is the neutron detector's basic readout circuit schematic for pulse amplification, adjustable detector bias, bias current compensation, pulse shaping and gain, analog output for pulse-height analysis, and "digital" output from a discriminator.

For testing, the preamps are plugged into a motherboard that provides power, an adjustable +0 to +30 V detector bias, bias current compensation, pulse shaping and gain, an analog output for pulse-height analysis, and a "digital" output from a discriminator. The dual-detector and motherboard are placed in a shielded box because the detectors are photosensitive. Bias current compensation is obtained using an integrator with a 0.1 s time constant to monitor the DC level of the input signal and thereby, feeding it back to the preamp for compensation. The input signal is processed by a pole-zero cancellation stage with a gain of -5.6 and time constants of 9.7 μs (zero) and 2 μs (pole). This is followed by an RC filter with a 2 μs time constant and an additional gain of +2. The discriminator output is a 3.3 V logic level that is "high" as long as the analog output is above threshold. The analog output is a semi-Gaussian pulse with a FWHM width of 6 μs and a gain of ~16 mV/fC. The input referred noise is 0.37 fC(rms) without bias current compensation and 0.49 fC(rms) with the compensation connected but without the effect of the bias current shot noise. All values were measured using a 100 pF detector capacitance.

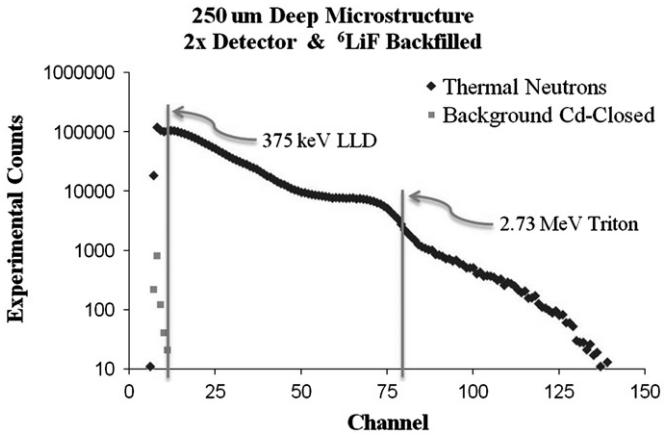

Fig. 5. Pulse height spectrum from conformal-diffused diode dual-integrated detector with 250 μm deep strait trench microstructures, showing response with and without (Cd shutter closed) neutrons. Electronic signal integration time was 2 μs.

3. Performance of dual-integrated neutron detector

The dual-integrated neutron counting efficiency was measured with a 0.0253 eV diffracted neutron beam from the Kansas State University TRIGA Mark II nuclear reactor. The neutron flux was calibrated with a Reuter–Stokes ^{3}He gas-filled proportional detector and found to be $1.05 \pm 0.02 \times 10^4$ n cm^{-2} s^{-1}. Details of the calibration method can be found in Ref. [27]. A pulse height spectrum was collected from the dual-integrated microstructured detector in the diffracted neutron beam with and without a Cd shutter, thereby allowing the collection of responses with and without thermal neutrons. Prompt gamma-rays emitted from the thin Cd shutter appear in the spectrum as numerous pulses at low energy near the noise floor of the detector system (see Fig. 5). The neutron counting efficiency was calculated by dividing the summed neutron counts, collected from the dual-detector with a lower level discriminator (LLD) set above the system noise, by the calibrated flux determined with the ^{3}He detector.

Fig. 5 shows the measured pulse height spectrum from the dual-integrated device, with each detector chip having 250 μm

deep trenches. The single dual-integrated device works well with as little as 2 V of applied bias. The leakage current for the 1 cm^2 dual-integrated devices was 500 nA/cm^2. The conformal device leakage current has been shown to be almost 2 orders of magnitude lower than the leakage current at the same voltage for the selective diffused etched device [26]. The pulse height spectrum shows many more counts than previously reported in single and dual-integrated devices [28]. Notice that the spectrum shows a downward shift of the pulse height signal from the detector. Some of this shift may be due to an overall increase in capacitance of the stacked device, thereby reducing the pulse height signal from the detector. Similar to the other tested devices with the Cd shutter closed [27,28], the gamma-ray component was negligible at a LLD setting above channel 11. With the LLD set to channel 11 (375 keV), intrinsic efficiency was measured to be $37.0 \pm 0.6\%$.

Ultimately, deeper microstructured trenches and dual-integrated devices show a reduction in pulse height, which can decrease the n/γ ratio. Yet, in the present work, this pulse height shift does not appear to be severe. Note that the gamma-ray interactions within the device also diminish with deeper perforations (due to less interaction volume), thereby allowing for smaller LLD settings resulting in superior gamma-ray discrimination, which has been previously shown to be 3×10^{-6} n γ^{-1} at an LLD of 500 keV [27].

To better understand why the pulse height spectrum of deep microstructured devices shifts to lower energies, a simulation was created using the *Silvaco* TCAD software package [36] to inspect the effect of the electric fields generated by the conformal diffusion process and the time-response of a signal pulse. *Silvaco* TCAD is an industry standard set of software packages for semiconductor device modeling. The TCAD software calls on the ATLAS tool as a Poisson solver and additional tools such as DEVICE3D or BLAZE3D are invoked to handle the complexities of 3-dimensional geometries and time-transient simulations. The model geometry specifications were defined to mimic shallow boron diffusion within the device microstructure, thereby creating a conformal *pn* junction diode within deep trench microstructures on a high resistivity *n*-type Si substrate (10,000 Ω cm). A 3-dimensional portion of a microstructured diode device was constructed with trench depths of 50, 100, and 250μm and a potential solution was obtained with a 2 V reverse bias applied.

Within the diode structure, a single-event upset was defined with a cloud, 10 μm by 10 μm, of electron–hole pairs centered midway between the trenches and at a depth of 45 μm from the top surface of the structure in all three model variations. Initially, this may seem unrealistic, but the outward diffusion of charge from a compact ionization track to form a broad cloud is very rapid. Compared to the timescale of charge drifting to form a signal pulse, the transition from a track-like shape to a diffuse cloud will appear instantaneous. As a result, there is no need to define the shape of the ion track specifically; therefore, the charge cloud was defined very generically to represent any number of triton tracks having random directions that pass through this probable location. In fact with iterative transient computation, such extreme conditions can make the simulation unstable and inaccurate. The amount of charge utilized in the simulation was representative of the number of electron–hole pairs generated from the kinetic energy capture in the semiconductor from triton. However, typically in diode devices the time dependent response of the device does not depend greatly on the quantity of charge, but more on the established electric fields, carrier mobility, and lifetime. A time-transient solution was obtained, which revealed the current resulting at the top electrode of the device as a function of time, which includes the sudden appearance of this cloud.

It should be noted here that this simulation of charge transport is not intended to determine an absolute response for these microstructured diode neutron detectors. There are many variables that affect the total signal that is induced and observed. The simulation was utilized to examine the relative differences in behavior between varying trench depth geometries. The comparative behavior due to the established electric field distributions for varying trench depth designs holds merit not only for the silicon microstructured diode neutron detector but also for any charge induction scenario utilizing cup-shaped electrodes with this echelon of aspect ratios.

The electric potential solution within a 250 μm deep trenched device (see Fig. 6) shows that more voltage is dropped below the trench structure rather than in between the trenches. Even though the silicon material is depleted of charge between the trenches, a significant electric field is established only where the potential drops below the trenched structure. As a result of the low electric field region between the trenches, the ionized charge cloud stagnates. With the *p*-side of the junction surrounding the charge cloud on three sides, holes are drawn more readily to this nearby conductive layer. Conversely, the electrons have little motivation to drift toward the opposing electrode and do not form considerable signal until they find their way down to the

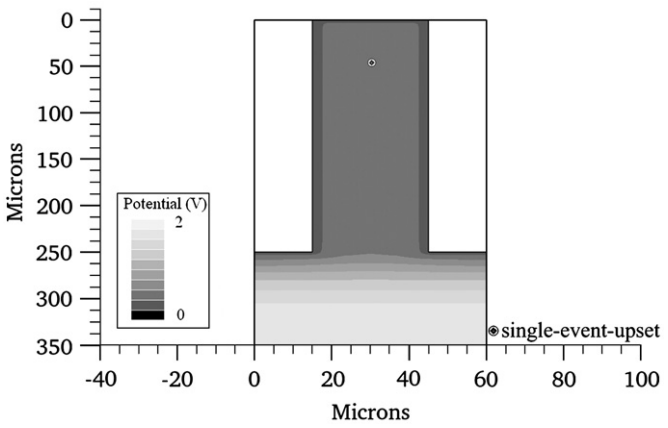

Fig. 6. Modeled electric potential solution within a 250 μm deep trenched device.

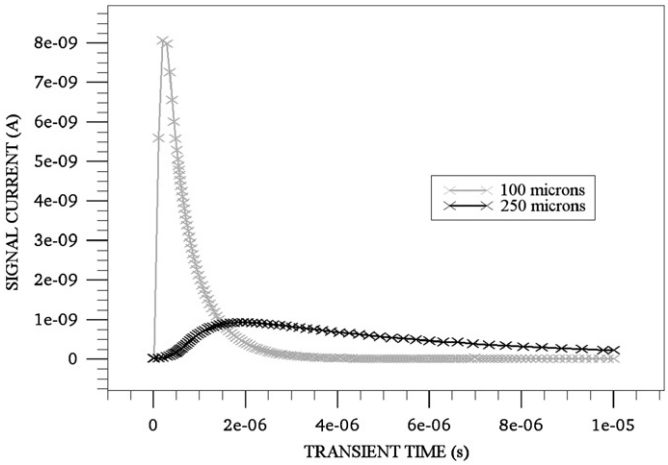

Fig. 7. Modeled transient solution of current versus time within 100 and 250 μm deep trenched devices.

high-electric field region below the trenches and are swept swiftly by the significant electric field. It is here that most of the signal is induced by electron transport.

The transient solution of current versus time correlates to this behavior. As the trenches become deeper from 100 μm to 250 μm, the time of current flow in the structure is drawn out over time. Similarly, the magnitude of current is reduced as the time to form a pulse is drawn out (See Fig. 7). In the case of 250 μm deep trenches it may take 10 μs to collect an entire signal pulse. Therefore, the electronic signal integration time for the dual-detector of 2 μs was not nearly long enough to accommodate the large integration time, which is due to the small electric potential in the Si microstructure, necessary to extract all the produced charge.

4. Conclusions

A dual-integrated, 1 cm^2 strait trench microstructured Si detector, backfilled with ^{6}LiF powder has been characterized for neutron sensitivity in a diffracted 0.0253 eV thermal neutron beam from a TRIGA Mark II nuclear reactor. An important clear advantage for the dual-integrated microstructured neutron detector design is the high efficiency achieved by appropriately stacking two detector chips into a single device. Efficiency is dramatically increased by capturing streaming neutrons from the first detector. The dual-integrated detector with two 250 μm deep trenched devices achieved 37% intrinsic efficiency. Finally, the gamma-ray rejection for the dual-integrated stacked device was high, with prompt Cd gamma-rays in the low energy to noise end of the pulse height spectrum, which is due to many combined effects explained in Ref. [7].

The improved fabrication design with *pn* junctions diffused within the microstructured trenches has lowered the leakage current and improved the pulse height signal from 50 and 100 μm devices [22] but when the trench depths are increased to 250 μm, the pulse height spectrum from the detector is shifted to the low energy end, which is most likely due to the short signal integration time circuit for the dual-detector stacked device. Because of this effect, future work will be dedicated to fabrication of interlaced microstructures that are etched from both sides of the Si diode, shown elsewhere [14], therefore, the electric field will be uniformly distributed across the Si detector volume and the signal integration time necessary to collect all the produced charge will be reduced and not limited by increased microstructure depth.

Acknowledgements

This work was supported in part by DTRA Contract DTRA-01-03-C-0051 and DOE Grant no. DE-FG07-04ID14599.

References

[1] R.A. Muminov, L.D. Tsvang, Sov. At. Energy 62 (1987) 255.
[2] J. Schelten, M. Balzhäuser, F. Höngesberg, R. Engels, R. Reinartz, Physica B (1997) 1084.
[3] J. Schelten, R. Reinartz, Neutron detector, US Patent 58804762, allowed March 9, 1999.
[4] C.P. Allier, in: Micromachined Si-well Scintillator Pixel Detectors, DUP Science, The Netherlands, 2001, pp. 132–133.
[5] J.K. Shultis, D.S. McGregor, in: Conference Record of the IEEE Nuclear Science Symposium, Rome, Italy, October 18–22, 2004, p. 4569.
[6] J.K. Shultis, D.S. McGregor, IEEE Trans. Nucl. Sci. NS-53 (2006) 1659.
[7] J.K. Shultis, D.S. McGregor, Nucl. Instr. and Meth. A 606 (2009) 608.
[8] D.S. McGregor, R.T. Klann, H.K. Gersch, E. Ariesanti, J.D. Sanders, B. Van Der Elzen, in: Conference Record of the IEEE Nuclear Science Symposium, San Diego, California, November 4–9, 2001, p. 2401.
[9] D.S. McGregor, R.T. Klann, H.K. Gersch, E. Ariesanti, J.D. Sanders, B.Van Der Elzen, IEEE Trans. Nucl. Sci. NS-49 (2002) 1999.
[10] D.S. McGregor, R.T. Klann, Pocked surface neutron detector, US Patent 6545281, allowed April 8, 2003.
[11] W.J. McNeil, S. Bellinger, T. Unruh, E. Patterson, A. Egley, D. Bruno, M. Elazegui, A. Streit, D.S. McGregor, in: Conference Record of the IEEE Nucl. Science Symposium, San Diego, CA, October 29–Nov. 3, 2006, p. 3732.
[12] D.S. McGregor, S. Bellinger, D. Bruno, W.L. Dunn, W.J. McNeil, E. Patterson, B.B. Rice, J.K. Shultis, T. Unruh, Radiat. Phys. Chem. 78 (2009) 874.
[13] C.J. Solomon, J.K. Shultis, W.J. McNeil, B.B. Rice, D.S. McGregor, Nucl. Instr. and Meth. A580 (2007) 326.
[14] D.S. McGregor, R.T. Klann, High-efficiency neutron detectors and methods of making the same, US Patent 7164138, allowed January 16, 2007.
[15] S.L. Bellinger, W.J. McNeil, T.C. Unruh, D.S. McGregor, in: IEEE Nuclear Science Symposium, Waikiki, Hawaii, October 28–November 3, 2007, p. 1904.
[16] D.S. McGregor, S.L. Bellinger, D. Bruno, W.J. McNeil, E. Patterson, J.K. Shultis, C.J. Solomon, T. Unruh, Proc. Soc. Photo-Opt. Instrum. Eng 6706 (2007) 0N1.
[17] D.S. McGregor, S. Bellinger, D. Bruno, W.J. McNeil, E. Patterson, B.B. Rice, in: Proceedings of the 32nd Annual GOMACTech Conference, Lake Buena Vista, FL, March 19–22, 2007.
[18] Q. Jahan, E. Patterson, B. Rice, W.L. Dunn, D.S. McGregor, Nucl. Instr. and Meth. B 263 (2007) 183.
[19] D.S. McGregor, S.L. Bellinger, W.J. McNeil, E.L. Patterson, B.B. Rice, J.K. Shultis, C.J. Solomon, US-patent pending, filed March 14, 2007.
[20] J. Uher, F. Frojdh, J. Jakubek, C. Kenney, Z. Kohout, V. Linhart, S. Parker, S. Petersson, S. Pospisil, G. Thungstrom, Nucl. Instr. and Meth. A576 (2007) 32.
[21] D.S. McGregor, J.K. Shultis, Proc. Soc. Photo-Opt. Instrum. Eng. 7079 (2008) 601.
[22] D.S. McGregor, S.L. Bellinger, W.J. McNeil, T.C. Unruh, in: Conference Record IEEE Nuclear Science Symposium, Dresden, Germany, October 19–25, 2008, p. 446.
[23] R.J. Nikolic, A.M. Conway, C.E. Reinhardt, R.T. Graff, T.F. Wang, N. Deo, C.L. Cheung, Appl. Phys. Lett. 93 (2008) 133502.
[24] A.M. Conway, T.F. Wang, N. Deo, C.L. Cheung, R.J. Nikolic, IEEE Trans. Nucl. Sci. NS-56 (2009) 2802.
[25] S.L. Bellinger, W.J. McNeil, T.C. Unruh, D.S. McGregor, IEEE Trans. Nucl. Sci. NS-56 (2009) 742.
[26] S.L. Bellinger, W.J. McNeil, D.S. McGregor, in: Proceedings of the MRS Symposium, vol. 1164, 2009.
[27] D.S. McGregor, W.J. McNeil, S.L. Bellinger, T.C. Unruh, J.K. Shultis, Nucl. Instr. and Meth. A 608 (2009) 125.
[28] S.L. Bellinger, W.J. McNeil, D.S. McGregor, in: IEEE Nuclear Science Symposium, Orlando, Florida, October 28–November 3, 2009, p. 986.
[29] R.V. Babcock, R.E. Davis, S.L. Ruby, K.H. Sun, E.D. Wolley, Nucleonics 17 (1959) 116.
[30] B. Feigl, H. Rauch, Nucl. Instr. and Meth. 61 (1968) 349.
[31] A. Rose, Nucl. Instr. and Meth. 52 (1967) 166.
[32] IAEA, biographical Series No. 18; Neutron Detectors, IAEA,Vienna, 1966 (references therein).
[33] D.S. McGregor, M.D. Hammig, Y.H. Yang, H.K. Gersch, R.T. Klann, Nucl. Instr. and Meth. A500 (2003) 272.
[34] K.E. Bean, IEEE Trans. Elect. Dev. ED-25 (1978) 1185.
[35] NIST Center for Neutron Research, Online, (2010, April). 〈http://www.ncnr.nist.gov/resources/n-lengths/elements/si.html〉.
[36] SILVACO, Online, (2010, January) 〈http://www.silvaco.com/〉.